Finite Elements in Analysis and Design 77 (2013) 31–39

Contents lists available at ScienceDirect

Finite Elements in Analysis and Design

journal homepage: www.elsevier.com/locate/finel

Stochastic stability analysis of steel tubes with random initial imperfections

Isaak Vryzidis [a], George Stefanou [a,b,*], Vissarion Papadopoulos [a]

[a] Institute of Structural Analysis & Antiseismic Research, School of Civil Engineering, National Technical University of Athens, 9 Iroon Polytechniou Street, Zografou Campus, 15780 Athens, Greece

[b] Institute of Structural Analysis & Dynamics of Structures, Department of Civil Engineering, Aristotle University of Thessaloniki, 54124 Thessaloniki, Greece

ARTICLE INFO

Article history:
Received 19 December 2012
Received in revised form
6 August 2013
Accepted 4 September 2013
Available online 11 October 2013

Keywords:
Shell finite element
Stochastic fields
Evolutionary spectrum
Random imperfections
Buckling load variability

ABSTRACT

In this paper, the effect of initial geometric imperfections on the buckling load of steel tubes (relatively thick cylindrical shells) under axial load and lateral pressure is investigated. The geometric imperfections are modeled as a 2D-1V non-homogeneous Gaussian stochastic field simulated using the spectral representation method. The evolutionary power spectrum of the non-homogeneous field is derived from available experimental measurements using the recently proposed method of separation. For the determination of the limit load variability of the tubes, a stochastic formulation based on Monte Carlo simulation is implemented. It is shown that the imperfections can lead to a substantial reduction of the buckling load and thus should be taken into account via a realistic description through stochastic field modeling.

1. Introduction

The failure of shell-type structures is often due to buckling phenomena mainly triggered by the initial geometric imperfections which occur during the manufacturing process. Therefore, the study of imperfect shell structures raised the interest of many researchers in the recent years. The main issues when dealing with this problem are the big discrepancy between theory and experiment as well as the large scatter in the measured buckling loads. Both deterministic and probabilistic approaches have been used to address the aforementioned issues. It was soon realized that a realistic approach to the problem could only be achieved by taking into account the inherent randomness of the imperfect geometries [10,15,18]. Buckling analysis based on such approach allows for a robust modeling of the buckling load scatter produced by different manufacturing processes as well as of the observed dispersion of experimental results [8,9,12].

Various methods have been developed to take into account the uncertainty in the geometry of the shell. Some methods use the Fourier series analysis of measured initial imperfections considering the series coefficients as random variables [5]. The idea of using two-dimensional Fourier series with random coefficients resulted from the analytical solution of the problem of stability of cylindrical shells which leads to the representation of buckling modes by series of this kind. These methods have in common that the limit load is computed analytically or semi-analytically. More recent research has proposed the use of stochastic fields to simulate the imperfections in conjunction with the finite element (FE) method to solve the stability problem [1–4,6,11,13,16,17,19–28,30–34].

The quality of the results obtained from the stochastic approach depends largely on the existence of data (experimental measurements) validating the assumptions made for the probabilistic characteristics (probability distribution, correlation structure) of the initial geometric imperfections. Many researchers have dealt with this issue in recent years. The result of their investigations has led to the conclusion that the variance does not remain constant in space and therefore the stochastic field describing the geometric imperfections cannot be considered homogeneous. In addition, the histograms of the computed buckling loads show that the probability density function is highly skewed and hence buckling loads follow a non-Gaussian distribution [9,23]. It is thus evident that the existence of databanks is important in order to avoid false assumptions and to achieve a realistic simulation of initial imperfections. In this framework, a novel approach has been recently proposed for the estimation of the evolutionary power spectra of non-homogeneous stochastic fields [26]. This approach, called "the method of separation", combines computational efficiency and accuracy as it achieves optimum simultaneous resolution in space and frequency domains.

* Correspondence to: School of Civil Engineering, National Technical University of Athens, Zografou Campus, 15780 Athens, Greece. Tel.: +30 2107722997.
E-mail address: stegesa@mail.ntua.gr (G. Stefanou).

0168-874X/$ - see front matter © 2013 Elsevier B.V. All rights reserved.
http://dx.doi.org/10.1016/j.finel.2013.09.002

In the present paper, the effect of initial (out-of-plane) geometric imperfections on the buckling load of steel tubes (relatively thick cylindrical shells) under axial load and external lateral pressure is investigated. The stability analysis of relatively thick steel tubes under external pressure is important, e.g. for the design and construction of offshore pipeline members [35,36]. The buckling behavior of this type of structures in presence of random imperfections has been studied very scarcely in the literature, in contrast to the case of thin cylindrical shells. Although relatively thick shells under pure axial loading are not imperfection sensitive, the simultaneous application of external lateral pressure results in a strongly unstable post-buckling path. The reason is that, even for thin tubes, the inelastic deformation, which occurs at the maximum moment locations, enables the formation of a plastic collapse mechanism. Tube stiffness is lost and the tube exhibits sudden collapse. An immediate consequence is the strong sensitivity of the response on the amplitude of the initial out-of-roundness [14].

The geometric imperfections are modeled as a 2D–1V non-homogeneous Gaussian stochastic field simulated using the spectral representation method [29]. The evolutionary power spectrum of the non-homogeneous field is derived from available experimental measurements [7] using the method of separation. For the determination of the limit load of the tubes, a stochastic finite element formulation based on Monte Carlo simulation (MCS) is implemented. Useful conclusions are derived regarding the effect of initial imperfections on buckling load variability and the necessity of using stochastic fields for a realistic representation of the imperfections is highlighted.

2. Modeling of random initial geometric imperfections

2.1. The method of separation

Out-of-plane initial geometric imperfections of shells are usually modeled as 2D non-homogeneous Gaussian stochastic fields. In this paper, the evolutionary power spectra of the non-homogeneous fields representing the initial geometric imperfections are derived from experimental measurements using the method of separation [26]. This method is based on simple principles of stochastic process theory. It is easy to implement, computationally efficient and at the same time accurate with optimum simultaneous resolution in space and frequency domains in contrast to the other existing methods [3,26].

The method of separation assumes that the available samples represent a separable zero-mean random field, thus the evolutionary power spectrum (EPS) can be decomposed into a frequency and a spatial part, which can be dealt with separately

$$S(\kappa,x)=S_h(\kappa)c_h(x) \tag{1}$$

An estimate $\tilde{S}_h(\kappa)$ of the homogeneous Fourier power spectrum in Eq. (1) can be obtained by the periodogram, where the integration over the frequency is done with a window as large as the sample length L

$$\tilde{S}_h(\kappa)=E\left[\frac{1}{2\pi L}\left|\int_0^L f^{(i)}(x)w(x-\frac{L}{2})e^{-I\kappa x}dx\right|^2\right] \tag{2}$$

Accordingly, an estimate $\tilde{c}_h(x)$ for the spatial envelope can be derived from the mean square of samples $f^{(i)}(x)$ as follows:

$$E[|f(x)|^2]=2\int_0^\infty S_h(\kappa)c_h(x)d\kappa=c_h(x)2\int_0^\infty S_h(\kappa)d\kappa \tag{3}$$

The estimate of the spatial envelope can then be obtained by replacing in Eq. (3) the analytical homogeneous spectrum $S_h(\kappa)$ and mean square $E[|f(x)|^2]$ by the corresponding estimates

$$\tilde{c}_h(x)=\frac{E[|f^{(i)}(x)|^2]}{2\int_0^\infty \tilde{S}_h(\kappa)d\kappa} \tag{4}$$

2.2. Representation of the imperfect geometry

The imperfect geometry of the tube is represented by the spatial variation of the radius of the structure as follows:

$$r(x,y)=R+a_0(x,y)+f(x,y) \tag{5}$$

where $r(x,y)$ is the varying initial radius at each point of the structure, R is the radius of the perfect cylinder, $a_0(x,y)$ is the mean function of the imperfections with respect to the perfect geometry of the tube and $f(x,y)$ is a zero-mean non-homogeneous Gaussian stochastic field. From the statistical analysis of the measured imperfections, it follows that the assumption of normality is in accordance with the experimental data.

The mean function $a_0(x,y)$ as well as the properties of stochastic field $f(x,y)$ are derived from a statistical analysis of experimentally measured imperfections on a group of six tubes, contained in a data bank of initial imperfections [7]. The geometric and material properties of these tubes are presented in Table 1. The average thickness, Young modulus and yield stress have been used in the analyses. A typical pattern of measured out-of-plane geometric imperfections is plotted in Fig. 1 for specimen 12A-3-1. The assumption of non-homogeneity of the imperfections is mainly based on the physical interpretation that imperfections are attributed to the manufacturing process where there is a basic mechanism creating an average imperfection pattern followed by a small scatter around this pattern. This is also verified in a number of publications on the topic [9,21,24,26], some of which involve a larger sample size. The mean function $a_0(x,y)$ is calculated via ensemble averaging at each point of the unfolded cylinder. A plot of $a_0(x,y)$ is presented in Fig. 2 where it can be observed that the mean value varies substantially along the two directions of the cylinder. At this point, it should be mentioned that, in order to be consistent with the assumption of a zero-mean random field used

Table 1
Experimental data of six imperfect tubes [7].

				Circumferential direction		Longitudinal direction	
Experiment	D/t	t (mm)	L (mm)	f_{ys} (kPa)	E (kPa)	f_{ys} (kPa)	E (kPa)
12A-3-1	96	6.5532	2413	2.64E+05	2.10E+08	2.69E+05	1.99E+08
12A-3-2	96	6.5024	2413	2.64E+05	2.10E+08	2.69E+05	1.99E+08
12A-3-3	96	6.4262	2413	2.56E+05	2.05E+08	2.66E+05	2.04E+08
12A-3–4	96	6.5024	2413	2.56E+05	2.05E+08	2.66E+05	2.04E+08
12A-3–5	96	6.477	2413	2.81E+05	2.05E+08	2.81E+05	2.02E+08
12A-3–6	96	6.5278	2413	2.81E+05	2.05E+08	2.81E+05	2.02E+08
Average		6.498167		E (kPa)	2.0417E+08		
				f_{ys} (kPa)	2.6950E+05		

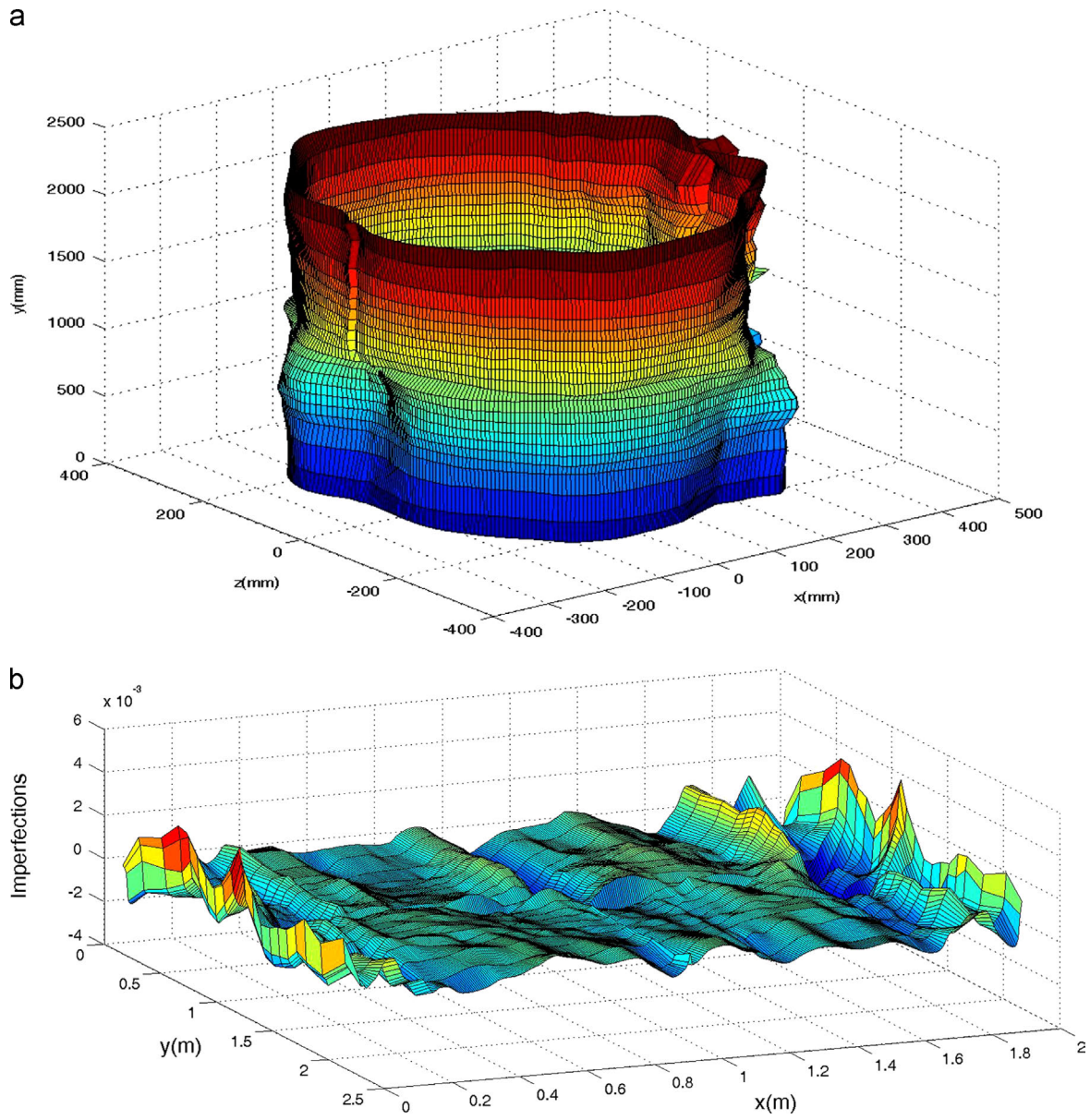

Fig. 1. (a) Tube 12A-3-1 with initial geometric imperfections and (b) Measured initial unfolded shape of (a).

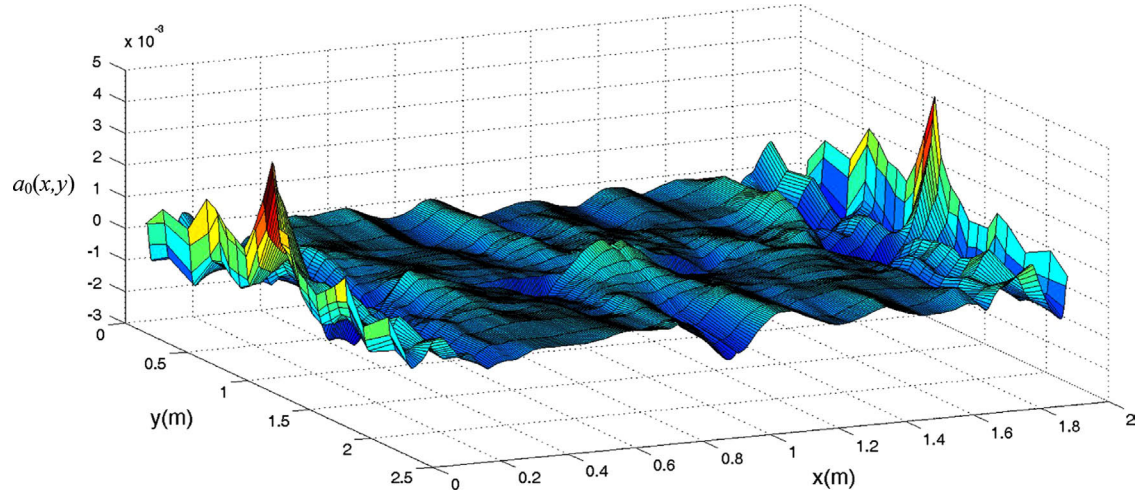

Fig. 2. Ensemble average of initial imperfections.

in the method of separation, the mean function $a_0(x,y)$ has been subtracted from each measured imperfection.

2.3. The spectral representation method

For the simulation of the non-homogeneous field $f(x,y)$ in Eq. (5), an evolutionary form of the spectral representation method is implemented. The EPS adopted in the present study is assumed to be uncoupled with respect to the axial and circumferential directions of the cylinder, as implied by the experimental measurements (refer to Fig. 1b). The assumption of spectral separability is valid for the case of geometric imperfections with narrow-band EPS, as shown in [24,26]. Therefore, the EPS of the stochastic field $f(x,y)$ can be written as follows:

$$S(\kappa_x,\kappa_y,x,y)=S_x(\kappa_x,x)S_y(\kappa_y,y) \tag{6}$$

where $S_x(\kappa_x,x)$ and $S_y(\kappa_y,y)$ are two independent 1D power spectra for the axial and circumferential direction, respectively. The two power spectra are obtained using the method of separation for 1D random fields described in Section 2.1 and are strongly narrow-band as shown in Fig. 3.

Using the EPS of Eq. (6), samples of the non-homogeneous imperfection field can be generated using the spectral representation method as follows:

$$f^{(i)}(x,y)=\sqrt{2}\sum_{n_1=0}^{N_1-1}\sum_{n_2=0}^{N_2-1}[A^{(1)}_{n_1n_2}\cos(\kappa_{1n_1}x+\kappa_{2n_2}y+\varphi^{(1)(i)}_{n_1n_2})+ +A^{(2)}_{n_1n_2}\cos(\kappa_{1n_1}x-\kappa_{2n_2}y+\varphi^{(2)(i)}_{n_1n_2})] \tag{7}$$

where $A^{(1)}_{n_1n_2}$, $A^{(2)}_{n_1n_2}$ depend not only on the wave numbers but also on the positions x, y

$$A^{(1)}_{n_1n_2}=\sqrt{2S(\kappa_{1n_1},\kappa_{2n_2},x,y)\Delta\kappa_1\Delta\kappa_2} \tag{8a}$$

$$A^{(2)}_{n_1n_2}=\sqrt{2S(\kappa_{1n_1},-\kappa_{2n_2},x,y)\Delta\kappa_1\Delta\kappa_2} \tag{8b}$$

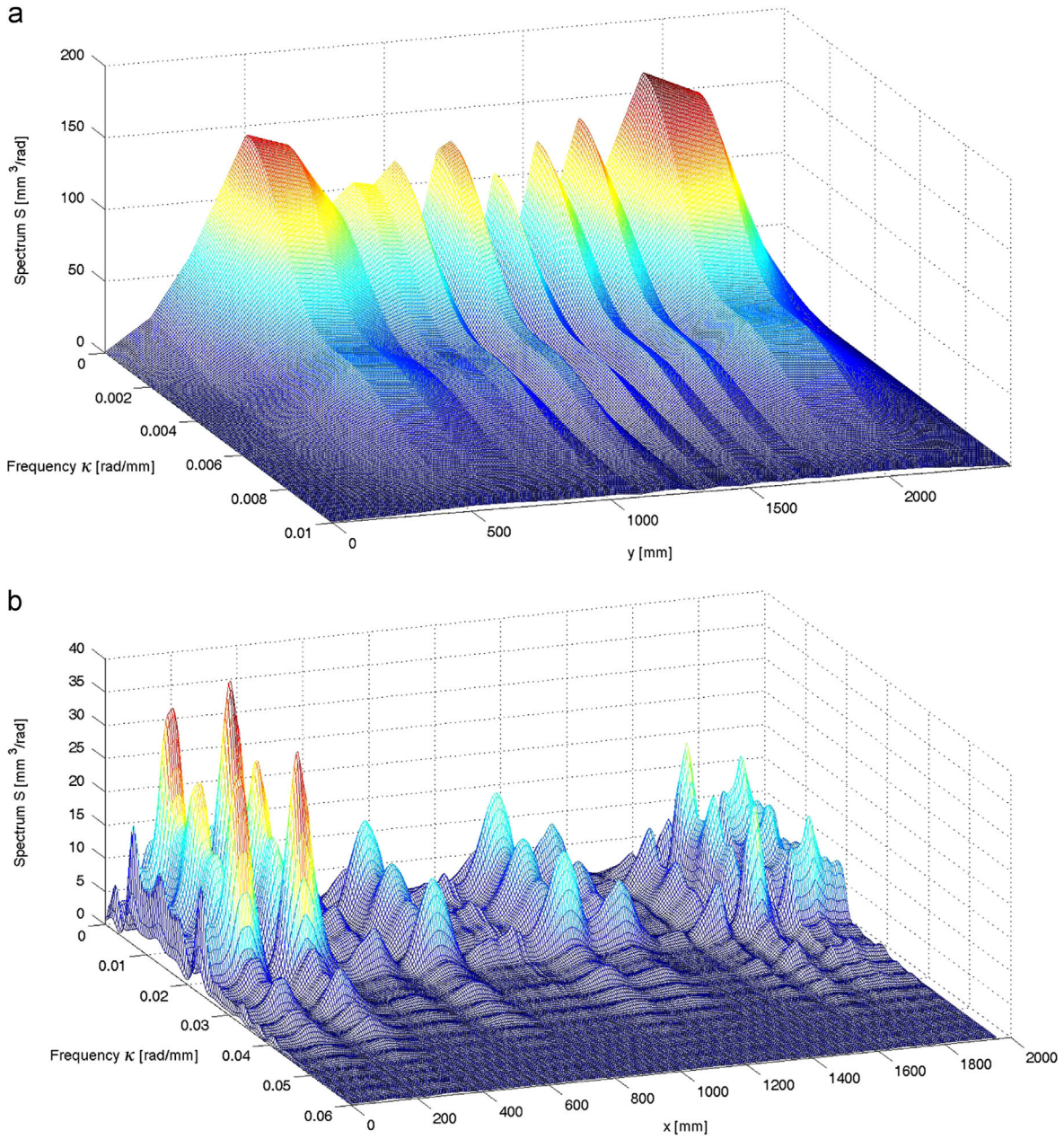

Fig. 3. Evolutionary power spectra along the: (a) axial direction and (b) circumferential direction of the tube.

and

$$\kappa_{1n_1} = n_1 \Delta\kappa_1 \quad \kappa_{2n_2} = n_2 \Delta\kappa_2 \tag{9}$$

$$\Delta\kappa_1 = \frac{\kappa_{1u}}{N_1} \quad \Delta\kappa_2 = \frac{\kappa_{2u}}{N_2} \tag{10}$$

$$n_1 = 0, 1, ..., N_1 - 1, \quad n_2 = 0, 1, ..., N_2 - 1 \tag{11}$$

The parameter κ_{ju}, $j=1, 2$, is a cut-off wave number defining the "active region" of the power spectral density function, beyond which the spectral power is supposed to be zero. $\varphi_{n_1 n_2}^{(j)(i)}$, $j=1, 2$, represent the realization for the (i) simulation of the independent random phase angles uniformly distributed in the range $[0,2\pi]$. A sample function of the initial geometric imperfections and the corresponding imperfect cylinder are depicted in Fig. 4. The comparison of Figs. 1 and 4 shows a very good agreement between measurements and simulations.

3. Summary of the proposed approach

The proposed approach comprises the following steps:

i. Numerical treatment of available experimental measurements of initial geometric imperfections.
ii. Use of the method of separation (Section 2.1) for the computation of the EPS of the imperfections.
iii. Generation of sample functions of the imperfections using the spectral representation method (imperfect tubes to be used in the analyses).

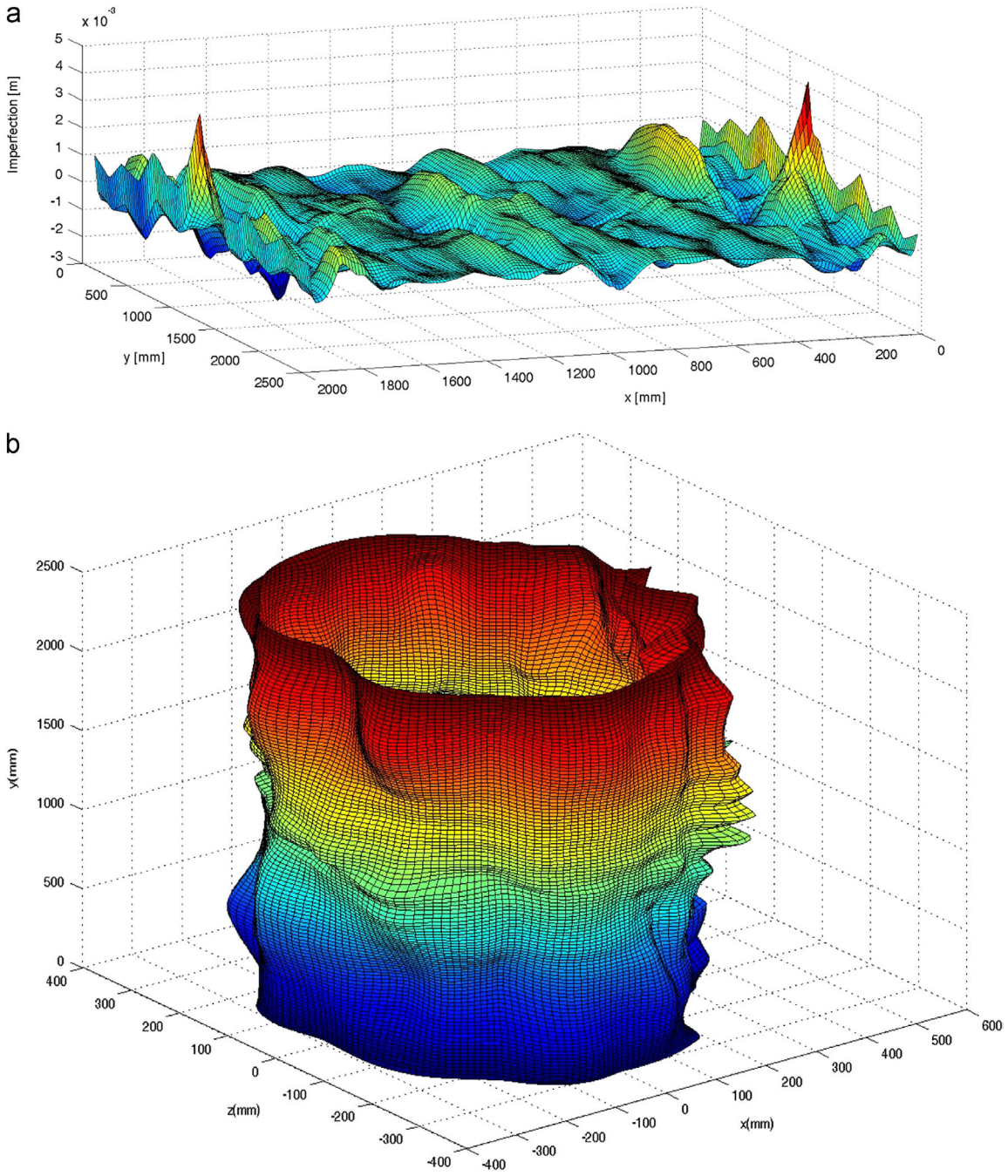

Fig. 4. (a) A sample function of the initial geometric imperfections generated using the spectral representation method and (b) the corresponding imperfect cylinder.

iv. Selection of FE mesh size. Mesh convergence studies are performed to define the appropriate mesh size for the analysis, which combines accuracy and computational efficiency.
v. Stochastic analysis of a number of imperfect tubes with different loading conditions (axial load, lateral pressure, combined axial load and lateral pressure) in the framework of MCS. In the nonlinear FE analyses performed, the load-displacement curve is obtained using a path-following strategy based on the arc-length method.
vi. Statistical treatment of the results: computation of buckling load variability.

4. Numerical examples

The mean material and geometric properties of the perfect cylinder are shown in Fig. 5 along with the bilinear stress–strain curve modeling the behavior of the material. The boundary conditions are specified as follows: the base edge nodes of the cylinder are fixed against all translations while the top edge nodes are free. As mentioned previously, mesh convergence studies are performed first in order to determine an optimum FE mesh size satisfying the following two requirements: (i) accurate prediction of the buckling load and (ii) accurate representation of the gradients of the stochastic initial imperfection field. Fig. 6 presents the results of such a convergence study of an imperfect cylinder under axial loading, for different mesh sizes. Although there are no significant differences in the computed buckling loads, the differences in the computational cost are substantial. For a 113×181

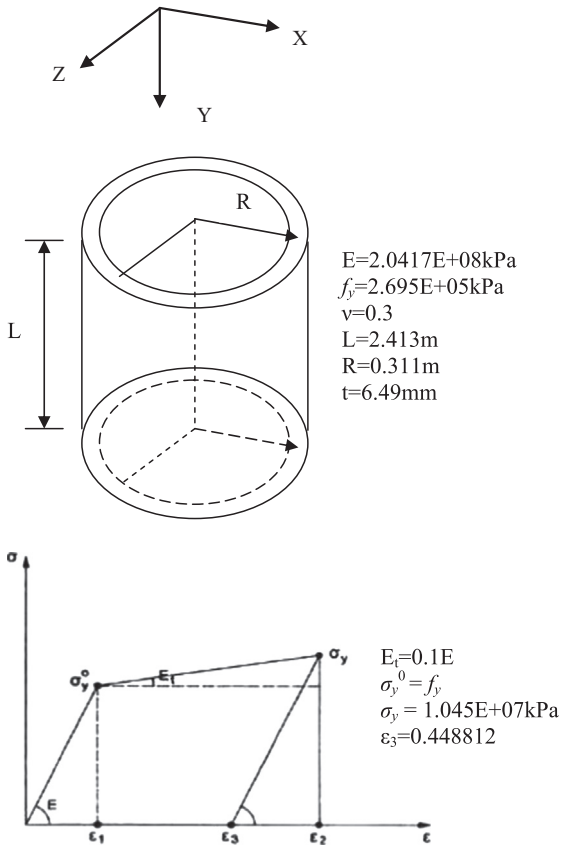

Fig. 5. Material and geometrical data of the perfect tube.

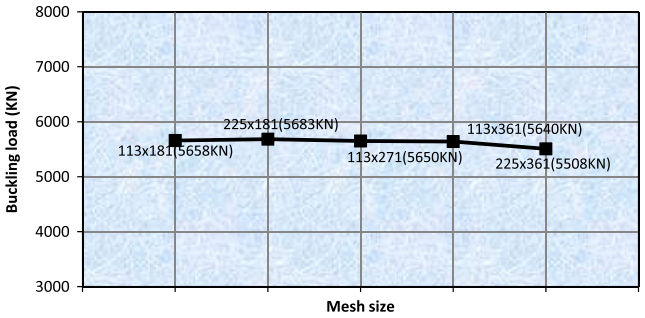

Fig. 6. Mesh convergence study for an imperfect tube under axial loading.

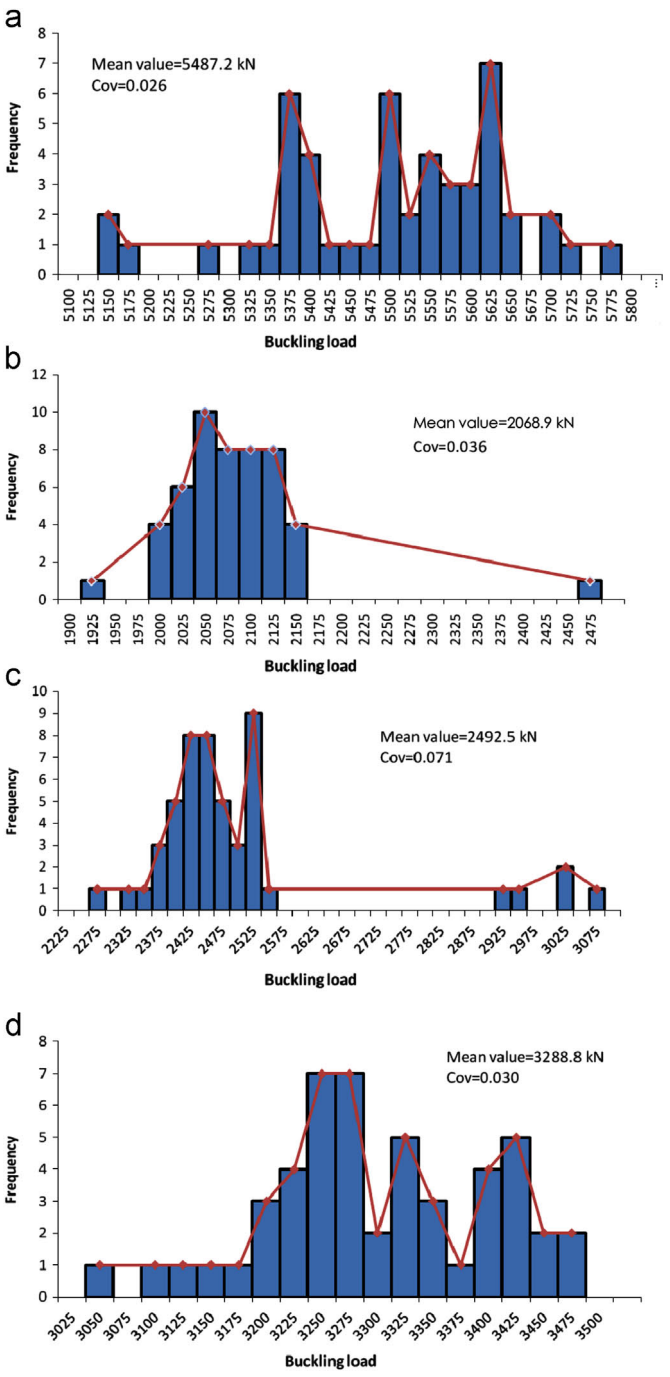

Fig. 7. Histograms of the computed buckling loads for different loading cases: (a) axial loading, (b) lateral pressure, (c) axial load/lateral pressure ratio = 1.25, and (d) axial load/lateral pressure ratio = 1.75.

mesh, the analysis required five times less computing time than that required for a 225×361 mesh. In addition, the average element size in the 113×181 mesh is smaller than a quarter of the periods of the stochastic field in the axial and circumferential directions corresponding to the upper cut-off frequency and thus provides sufficient accuracy. Therefore, the coarse mesh (113×181) will be used in the following analyses as it combines accuracy and computational efficiency.

Fifty tubes with initial geometric imperfections produced by the spectral representation method have been analyzed using the nonlinear FE approach mentioned in Section 3 for six different loading cases: axial load, lateral pressure, combined axial load and lateral pressure with ratio of 5, 2.5, 1.75 and 1.25. For comparison purposes, nonlinear FE analyses of the perfect cylinder have also been performed.

The histograms of the computed buckling loads P_u along with their mean value and coefficient of variation (Cov) are presented in Fig. 7 for the different loading cases examined. The form of the histograms is different and the scatter of buckling loads around the mean value is moderate. In the case of axial load/lateral pressure ratio equal to 1.25, the buckling load Cov reaches the value of 7%. The load–displacement curves for an imperfect cylinder and various loading combinations are shown in Fig. 8. It can be observed that the form of the load–displacement curve is highly sensitive to the ratio of axial load vs. lateral pressure. The limit load is reduced by increasing the lateral pressure (see also Fig. 7). In the case of pure axial compression, buckling is clearly elastoplastic and becomes gradually a bifurcation-type elastic one as external pressure increases.

The failure modes of a randomly selected imperfect tube for three of the six loading cases mentioned above are depicted in Fig. 9. It can be observed that the failure modes are affected significantly by the type of loading. There are three local buckles for axial load/lateral pressure ratio equal to 2.5 and only one local buckle for pure lateral pressure, indicating the complexity of the buckling phenomenon. It is also evident that local buckling is occurring in all loading cases. These observations confirm the importance of initial geometric imperfections which are responsible for the different failure modes.

The significance of initial geometric imperfections is further highlighted through comparisons with the buckling behavior of the perfect tube obtained also with nonlinear FE analysis. Table 2 shows the lateral pressure and the corresponding limit load of the perfect tube. It can be observed that the limit (axial) load is much larger than that resulting from the stochastic analysis of the imperfect cylinders. Furthermore, by increasing the lateral pressure, the limit load increases instead of decreasing. However, the opposite happens in the imperfect cylinder where the limit load decreases with the lateral pressure (see Fig. 8). Therefore, the presence of initial geometric imperfections cannot be neglected. The failure modes of the perfect tube are depicted in Fig. 10 for different loading cases. In the case of pure axial load (Fig. 10a), it is observed that the deformations are concentrated at the upper and lower ends of the cylinder, which is in contrast to the results

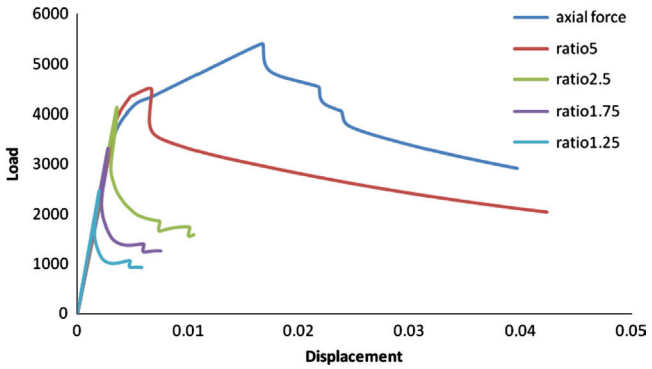

Fig. 8. Load–displacement curves for an imperfect cylinder and various loading combinations.

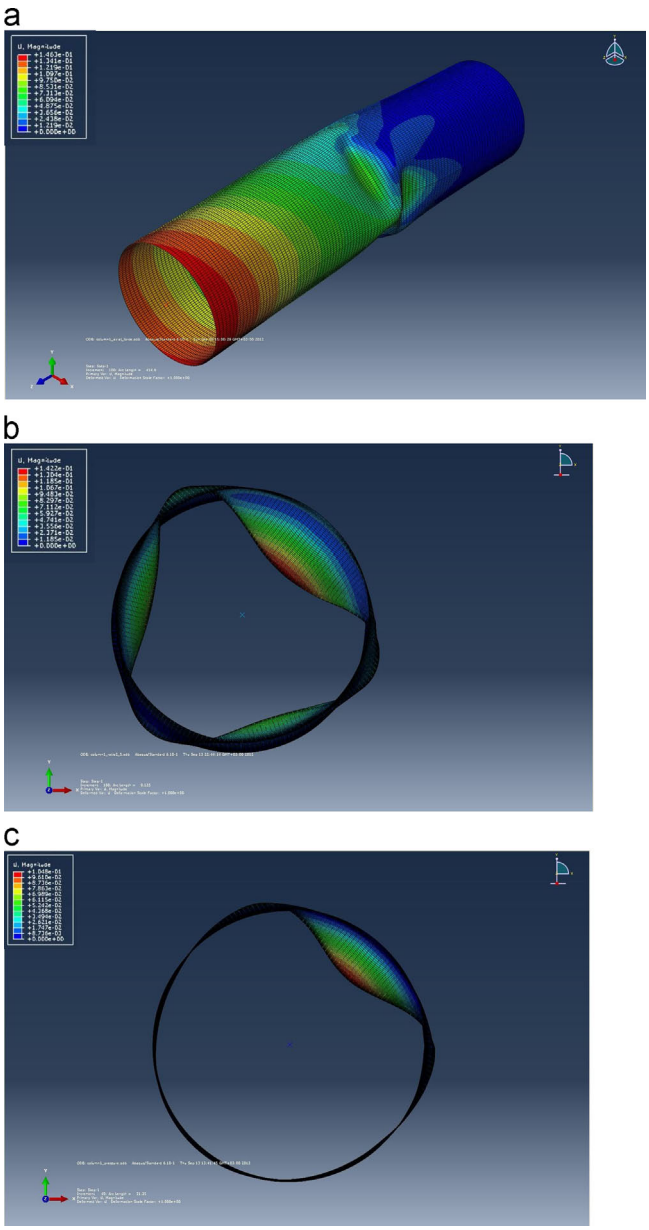

Fig. 9. Failure modes of a randomly selected imperfect tube for three loading cases: (a) axial loading, (b) axial load/lateral pressure ratio=2.5, and (c) lateral pressure.

Table 2
Applied lateral pressure and corresponding limit load of the perfect cylinder.

	Limit load P_u (kN)	Lateral pressure (kPa)
Pure axial load	7747.69	0.00
Ratio 5	7873.60	1574.72
Ratio 2.5	8535.58	3414.23
Ratio 1.75	8684.92	4962.81
Ratio 1.25	8205.93	6564.74
Pure lateral pressure	0.00	42120.80

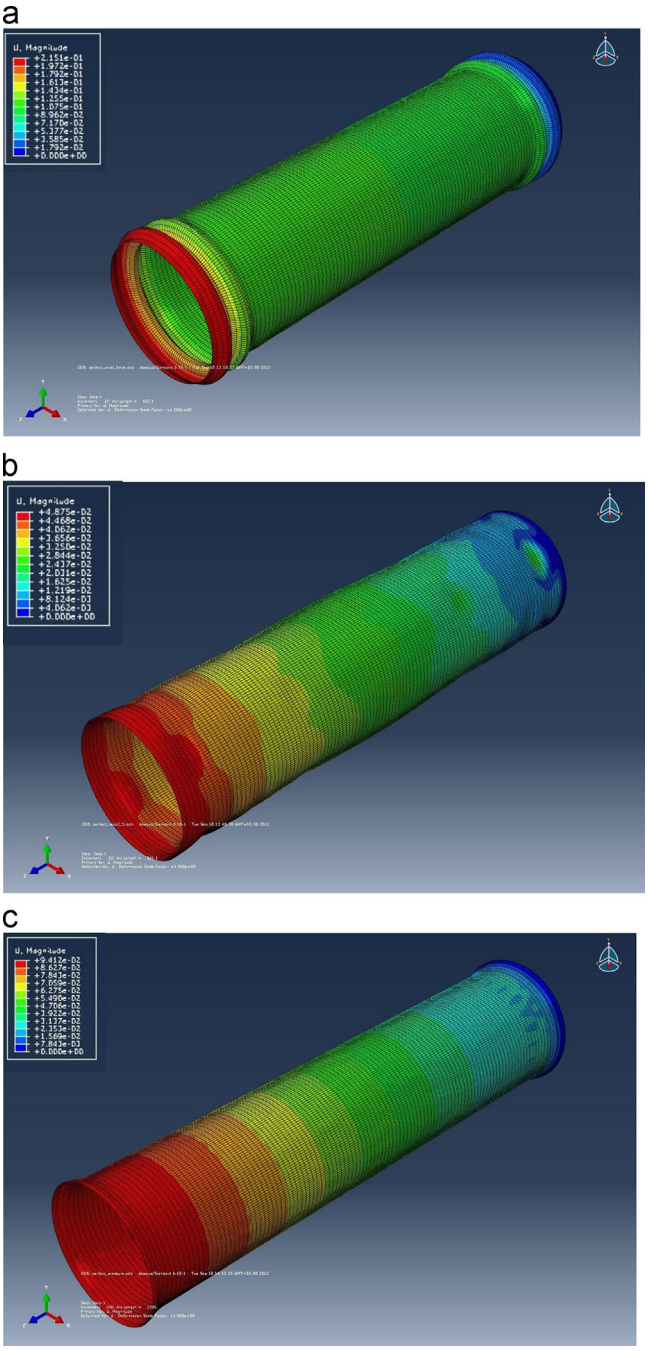

Fig. 10. Failure modes of the perfect tube for three loading cases: (a) axial loading, (b) axial load/lateral pressure ratio=2.5, and (c) lateral pressure.

obtained from the stochastic analyses (see Fig. 9). For pure lateral pressure (Fig. 10c), the perfect cylinder seems not to buckle unless a small defect is introduced to the geometry that leads to some kind of buckling initiation (Fig. 9). For axial load/lateral pressure ratio equal to 2.5 (Fig. 10b), a local buckling occurs near the ends of the cylinder and the failure mode is again substantially different to that of the imperfect structure.

Finally, the stochastic interaction diagram is shown in Fig. 11. The minimum and maximum values of the computed limit loads are presented in the same diagram along with the mean value for comparison purposes. It is evident that the variability is substantial especially for large lateral pressure which also leads to significant reduction of the buckling load.

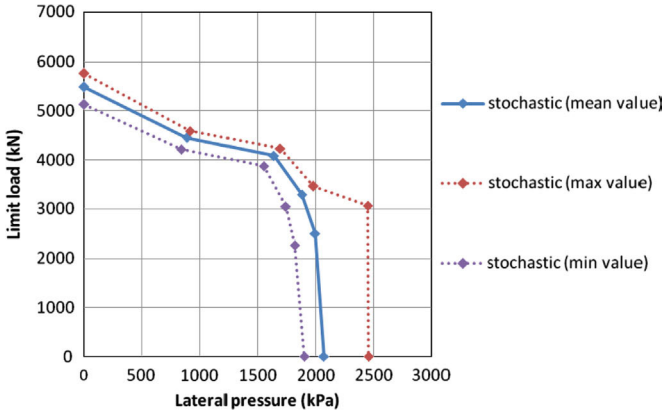

Fig. 11. Stochastic interaction diagram of the imperfect tubes.

5. Conclusions

In this paper, the effect of initial geometric imperfections on the buckling load of steel tubes under axial load and external lateral pressure was investigated. As demonstrated by the numerical investigations and the experimental results, the imperfections can lead to a substantial reduction of the buckling load and thus should be taken into account via a realistic description through stochastic field modeling. The buckling load variability due to the presence of initial imperfections is moderate. The failure modes of the tubes are significantly affected by the type of loading and the imperfections. In the case of pure axial loading, local buckling occurs near the middle of the imperfect tube, which is in contrast to the results obtained for the perfect structure where “elephant foot” buckling occurs. The effect of the variability of other mechanical properties such as the thickness of the tube and the yield stress of the material on the buckling load will be the subject of future work.

Acknowledgment

This work has been partially supported by the research project “Stochastic stability analysis of elastoplastic cylindrical shells” (PEBE 2010) of the National Technical University of Athens. This support is gratefully acknowledged. Special thanks are also due to Professor S.A. Karamanos for providing the experimental data on the imperfect steel tubes.

References

[1] J. Arbocz, The effect of imperfect boundary conditions on the collapse behavior of anisotropic shells, International Journal of Solids and Structures 37 (2000) 6891–6915.
[2] E. Bielewicz, J. Górski, Shells with random geometric imperfections: simulation-based approach, International Journal of Non-Linear Mechanics 37 (4-5) (2002) 777–784.
[3] M. Broggi, G.I. Schuëller, Efficient modeling of imperfections for buckling analysis of composite cylindrical shells, Engineering Structures 33 (5) (2011) 1796–1806.
[4] C.K. Choi, H.C. Noh, Stochastic analysis of shape imperfections in rc cooling tower shells, Journal of Structural Engineering (ASCE) 126 (3) (2000) 417–423.
[5] M.K. Chryssanthopoulos, C. Poggi, Stochastic imperfection modeling in shell buckling studies, Thin-Walled Structures 23 (1995) 179–200.
[6] K.J. Craig, W.J. Roux, On the investigation of shell buckling due to random geometrical imperfections implemented using Karhunen–Loève expansions, International Journal for Numerical Methods in Engineering 73 (2008) 1715–1726.
[7] Eder, M.F., Grove, R.B., Peters, S.W., Miller, C.D., Collapse tests of fabricated cylinders under combined axial compression and external pressure, Final Report, CBI Industries, Inc., 1984.
[8] I. Elishakoff, Probabilistic resolution of the twentieth century conundrum in elastic stability, Thin-Walled Structures 59 (2012) 35–57.

[9] I. Elishakoff, Y.W. Li, J.H. Starnes Jr., Non-Classical Problems in the Theory of Elastic Stability, Cambridge University Press, Cambridge, UK, 2001.
[10] W.B. Fraser, B. Budiansky, The buckling of a column with random initial deflections, Journal of Applied Mechanics (ASME) 36 (1969) 233–240.
[11] L.L. Graham, E.F. Siragy, Stochastic finite element analysis for elastic buckling of stiffened panels, Journal of Engineering Mechanics (ASCE) 127 (1) (2001) 91–97.
[12] K. Ikeda, K. Murota, Asymptotic and probabilistic approach to buckling of structures and materials, Applied Mechanics Reviews (ASME) 61 (2008) 040801. (16 pp.).
[13] M.M. Kamiński, P. Swita, Generalized stochastic finite element method in elastic stability problems, Computers and Structures 89 (11-12) (2011) 1241–1252.
[14] Karamanos, S.A., Papadimitriou, C., 2000. Sensitivity of inelastic tube collapse on initial imperfections: a probabilistic approach, in: Proceedings of the Fourth International Colloquium on Computation of Shell and Spatial Structures, Chania-Crete, Greece, 4–7 June 2000.
[15] W.T. Koiter, The effects of axisymmetric imperfections on the buckling of cylindrical shells under axial compression, Proceedings of Royal Netherlands Academy of Sciences 66 (B) (1963) 265–279.
[16] H.C. Noh, Effect of multiple uncertain material properties on the response variability of in-plane and plate structures, Computer Methods in Applied Mechanics and Engineering 195 (19-22) (2006) 2697–2718.
[17] A.K. Onkar, C.S. Upadhyay, D. Yadav, Generalized buckling analysis of laminated plates with random material properties using stochastic finite elements, International Journal of Mechanical Sciences 48 (7) (2006) 780–798.
[18] G.V. Palassopoulos, New approach to buckling of imperfection-sensitive structures, Journal of Engineering Mechanics (ASCE) 119 (1993) 850–869.
[19] V. Papadopoulos, D.C. Charmpis, M. Papadrakakis, A computationally efficient method for the buckling analysis of shells with stochastic imperfections, Computational Mechanics 43 (2008) 687–700.
[20] V. Papadopoulos, M. Papadrakakis, Finite element analysis of cylindrical panels with random initial imperfections, Journal of Engineering Mechanics (ASCE) 130 (8) (2004) 867–876.
[21] V. Papadopoulos, M. Papadrakakis, The effect of material and thickness variability on the buckling load of shells with random initial imperfections, Computer Methods in Applied Mechanics and Engineering 194 (12–16) (2005) 1405–1426.
[22] V. Papadopoulos, G. Soimiris, M. Papadrakakis, Buckling αnalysis of I-section portal frames with stochastic imperfections, Engineering Structures 47 (2013) 54–66.
[23] V. Papadopoulos, G. Stefanou, M. Papadrakakis, Buckling analysis of imperfect shells with stochastic non-Gaussian material and thickness properties, International Journal of Solids and Structures 46 (2009) 2800–2808.
[24] C.A. Schenk, G.I. Schuëller, Buckling analysis of cylindrical shells with random geometric imperfections, International Journal of Non-Linear Mechanics 38 (7) (2003) 1119–1132.
[25] C.A. Schenk, G.I. Schuëller, Buckling analysis of cylindrical shells with cut-outs including random boundary and geometric imperfections, Computer Methods in Applied Mechanics and Engineering 196 (35–36) (2007) 3424–3434.
[26] D. Schillinger, V. Papadopoulos, Accurate estimation of evolutionary power spectra for strongly narrow-band random fields, Computer Methods in Applied Mechanics and Engineering 199 (2010) 947–960.
[27] D. Schillinger, V. Papadopoulos, M. Bischoff, M. Papadrakakis, Buckling analysis of imperfect I-section beam-columns with stochastic shell finite elements, Computational Mechanics 46 (2010) 495–510.
[28] S. Shang, G.J. Yun, Stochastic finite element with material uncertainties: implementation in a general purpose simulation program, Finite Elements in Analysis and Design 64 (2013) 65–78.
[29] M. Shinozuka, G. Deodatis, Simulation of multi-dimensional gaussian stochastic fields by spectral representation, Applied Mechanics Reviews (ASME) 49 (1) (1996) 29–53.
[30] G. Stefanou, The stochastic finite element method: past, present and future, Computer Methods in Applied Mechanics and Engineering 198 (2009) 1031–1051.
[31] G. Stefanou, Response variability of cylindrical shells with stochastic non-Gaussian material and geometric properties, Engineering Structures 33 (2011) 2621–2627.
[32] G. Stefanou, V. Papadopoulos, M. Papadrakakis, Buckling load variability of cylindrical shells with stochastic imperfections, International Journal of Reliability and Safety 5 (2011) 191–208.
[33] C.J. Stull, J.M. Nichols, C.J. Earls, Stochastic inverse identification of geometric imperfections in shell structures, Computer Methods in Applied Mechanics and Engineering 200 (25–28) (2011) 2256–2267.
[34] M. Tootkaboni, L. Graham-Brady, B.W. Schafer, Geometrically non-linear behavior of structural systems with random material property: an asymptotic spectral stochastic approach, Computer Methods in Applied Mechanics and Engineering 198 (2009) 3173–3185.
[35] N.G. Tsouvalis, A.A. Zafeiratou, V.J. Papazoglou, The effect of geometric imperfections on the buckling behavior of composite laminated cylinders under external hydrostatic pressure, Composites Part B: Engineering 34 (2003) 217–226.
[36] M.K. Yeh, S. Kyriakides, On the collapse of inelastic thick-walled tubes under external pressure, Journal of Energy Resources Technology, Transactions of the ASME 108 (1) (1986) 35–47.